2015-09

Fidelity of low-frequency underwater acoustic measurements by sensors mounted on compact platforms

Godin, Oleg A.

Acoustical Society of America

Godin, Oleg A. "Fidelity of low-frequency underwater acoustic measurements by sensors mounted on compact platforms." The Journal of the Acoustical Society of America 146.5 (2019): EL405-EL411.
http://hdl.handle.net/10945/66480

Fidelity of low-frequency underwater acoustic measurements by sensors mounted on compact platforms

Oleg A. Godin
Physics Department, Naval Postgraduate School, Monterey, California 93943, USA
oagodin@nps.edu

Abstract: Measurements by sensors mounted on compact platforms are affected by sound scattering from the platform. Assuming a spherical shape of the platform, this paper investigates the differences between the ambient and measured characteristics of low-frequency signals and noise for scalar and vector sensors. In the near field of the platform, low-frequency perturbations in oscillatory velocity are generally much larger than pressure perturbations. These perturbations prevent mounted vector sensors from correctly measuring the direction of the free-field oscillatory velocity. The feasibility of a compensation of the distortions in scalar and vector sensor measurements is discussed.

[CCC]
Date Received: August 23, 2019 **Date Accepted:** October 4, 2019

1. Introduction

Aside from self-noise,[1] measured acoustic quantities deviate from their ambient values because of the sound diffraction by, or scattering from, the platform used to deploy the sensors in the water column. In underwater acoustics, the relation between ambient fields and the measurements made with mounted hydrophones[2,3] and vector sensors[4–7] is usually studied with the platform modeled as an infinite plane or a layered structure. This is a good approximation at high- and mid-frequencies and for hull-mounted sensors. However, at the low frequencies of primary interest in noise interferometry[8–10] and seismo-acoustics,[4,11] the entire platform may be small compared to the wavelength. The platform may be acoustically compact even at mid-frequencies, when sensors are carried by gliders or autonomous underwater vehicles. The goal of this Letter is to investigate theoretically, in a geometrically simple setting that admits an analytic treatment, the relation between ambient acoustic fields and measurements made by various sensors mounted on a compact platform.

2. Theory

Consider the effect of a spherical float of radius a on the acoustic field in its vicinity. Introduce Cartesian (x, y, z) and spherical r, θ, φ coordinates with origin at the center of the float [Fig. 1(a)]. The polar angle θ is measured from the positive direction of the z coordinate axis. Let the plane monochromatic sound wave $p_{in} = D\exp(-ikz)$ be incident on the mooring. Here p, D, $k = \omega/c$, ω, and c are the acoustic pressure, incident wave amplitude, wavenumber, wave frequency, and sound speed. Time dependence $\exp(-i\omega t)$ of the acoustic field is assumed and suppressed. The acoustic pressure, radial v_r and tangential v_t components of the oscillatory velocity $\mathbf{v} = \nabla p/i\omega\rho$ at $r \geq a$ are given by a sum of partial waves (spherical harmonics),[12–15]

$$p = D\sum_{n=0}^{\infty}(2n+1)(-i)^n P_n(\cos\theta)B_n(kr), \quad B_n(q) = j_n(q) - A_n h_n^{(1)}(q), \tag{1}$$

$$v_r = \frac{-iD}{\rho c}\sum_{n=0}^{\infty}(2n+1)(-i)^n P_n(\cos\theta)B_n'(kr), \tag{2}$$

$$v_t = \frac{-iD}{\omega\rho r}\sum_{n=1}^{\infty}(2n+1)(-i)^n B_n(kr)\frac{\partial}{\partial\theta}P_n(\cos\theta). \tag{3}$$

Here prime denotes derivative of the function with respect to its argument; ρ is water density; P_n, j_n, and $h_n^{(1)}$ are Legendre polynomials, spherical Bessel functions, and spherical Hankel functions of the first kind.[16] Because of the axial symmetry of the problem, acoustic field is independent of the azimuthal angle φ, and the tangential velocity has no azimuthal component.

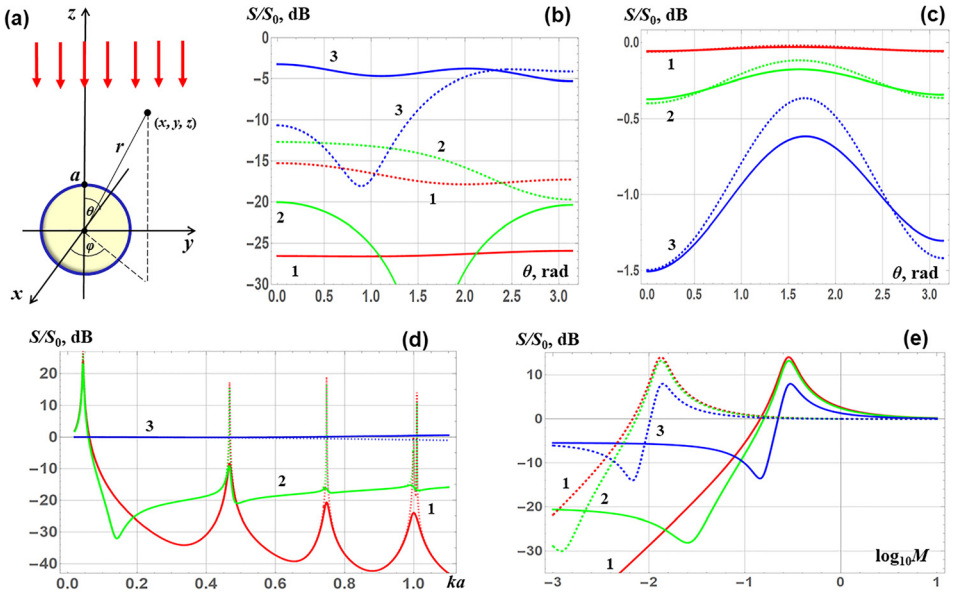

Fig. 1. (Color online) Acoustic pressure on a mounted hydrophone. (a) Geometry of the problem. Receiver is located at point (x, y, z) in the vicinity of a spherical platform (float). (b) Angular dependence of the power spectrum distortion for an incident plane wave. The ratio of the measured, S, and ambient, S_0, power spectra is shown for a gas-filled float ($M = 0.013$, $s = 2/9$) at $ka = 0.2$ (curves 1), 0.5 (2), and 1.0 (3) and $r/a = 1$ (solid lines) and $r/a = 1.2$ (dashed lines). (c) Same as (b) but for a syntactic-foam-type float ($M = 0.5$, $s = 1.5$). (d) Frequency dependence of the distortion of the power spectrum of isotropic noise. Ratio of the measured and ambient power spectra is shown for a gas-filled float ($M = 0.013$, $s = 2/9$) at $r/a = 1.0$ and 1.1 (curves 1 and 2, respectively) with (solid lines) and without (dashed lines) account for sound absorption in the float. Curves 3 refer to a flush-mounted hydrophone ($r = a$) on a denser platform with $s = 1.5$ and $M = 0.5$ (dotted line) or $M = 10$ (solid line). (e) Same as (d) but without absorption and for a wide range of platform densities at $r/a = 1.0$ (curves 1), 1.3 (2), and 2.0 (3) at $ka = 0.2$ and $s = 2/9$ (solid lines) or 1 (dashed lines).

Coefficient A_n in Eq. (1) has the meaning of amplitude of the n-th spherical harmonic of the scattered wave and depends on the parameters of the float; the infinite sums in Eqs. (1)–(3) give the incident wave when $A_n = 0$ for all n. For a float modeled as a fluid sphere with density $\rho_1 = M\rho$ and sound speed $c_1 = sc$, scattering amplitudes A_n are[12,14,15]

$$A_n = \frac{Msj_n'(ka)j_n(ka/s) - j_n(ka)j_n'(ka/s)}{Msh_n^{(1)\prime}(ka)j_n(ka/s) - h_n^{(1)}(ka)j_n'(ka/s)}. \tag{4}$$

Absolute value of the scattering amplitude does not exceed 1 and reaches its maximum at resonances frequencies, where the imaginary part of the denominator in the right side of Eq. (4) vanishes and $A_n = 1$.[12,15]

At low frequencies, when radius of the sphere is small compared to the acoustic wavelength inside and outside the float, $(1 + s^{-1})ka \ll 1$ and Eq. (4) can be simplified,[15]

$$A_0 \approx \frac{i(1 - Ms^2)(ka)^3}{(1 - ika)k^2a^2 - 3Ms^2}, \quad A_n \approx -i\left[\frac{2^n n!}{(2n)!}\right]^2 \frac{n(ka)^{2n+1}(M-1)}{(Mn + M + n)(2n+1)}, \quad n = 1, 2, \ldots. \tag{5}$$

Equation (5) shows that scattering amplitudes are small and rapidly decrease with n when $n \geq 1$. $|A_0| \ll 1$ as well, except in the vicinity of the frequency of Minnaert (or "bubble") resonance, which occurs at $k^2a^2 = 3Ms^2$, if $Ms^2 \ll 1$, i.e., when the float is much more compressible than water.

In addition to the signal, sound scattering by a platform affects underwater noise. To model ambient noise on a mounted sensor, Eqs. (1)–(3) should be averaged according to free-field directivity of ambient noise. In particular, ambient noise that is isotropic in the absence of platform can be modeled as a superposition of random incident plane waves with the acoustic pressure variance $|D^2|$ per unit solid angle, with waves coming from different directions being incoherent and having equal root-mean-square (RMS) amplitudes. Then, the variance of the response of a mounted sensor is obtained by incoherent averaging over the entire 4π solid angle of the response to an incident plane wave. Taking into account the orthogonality relations[16]

$$\int_0^\pi P_n(\cos\theta)P_m(\cos\theta)\sin\theta d\theta = \frac{1}{m(m+1)}\int_0^\pi \frac{\partial P_n(\cos\theta)}{\partial\theta}\frac{\partial P_m(\cos\theta)}{\partial\theta}\sin\theta d\theta = \frac{2\delta_{mn}}{2m+1}, \tag{6}$$

of Legendre polynomials $P_n(\cos\theta)$ and associated Legendre polynomials $\partial P_n(\cos\theta)/\partial\theta$, we obtain from Eqs. (1)–(3)

$$\langle|p^2|\rangle = |D^2|\sum_{n=0}^{\infty}(2n+1)|B_n^2(kr)|, \tag{7}$$

$$\langle|v_r^2|\rangle = \frac{|D^2|}{\rho^2c^2}\sum_{n=0}^{\infty}(2n+1)|B_n'(kr)|^2, \quad \langle|v_t^2|\rangle = \frac{|D^2|}{\omega^2\rho^2r^2}\sum_{n=1}^{\infty}n(n+1)(2n+1)|B_n^2(kr)|. \tag{8}$$

In Eq. (6), the Kronecker delta δ_{mn} equals 0 if $m \neq n$ and 1 if $m=n$.

At low frequencies, for the response of a mounted hydrophone to an incident plane wave or isotropic noise we find, respectively,

$$p = D\left(e^{-ikr\cos\theta} - A_0 + \frac{iA_0}{kr} + \frac{3A_1\cos\theta}{k^2r^2}\right), \quad \langle|p^2|\rangle = |D^2|\left|1 - A_0 + \frac{iA_0}{kr}\right|^2 \tag{9}$$

from Eqs. (1), (5), and (7). In derivation of Eq. (9) we assumed $kr \ll 1$, used the small-argument approximations[16] $j_n(q) \sim 2^n n!q^n/(2n+1)!$, $h_n^{(1)}(q) \sim -i(2n)!/2^n n!q^{n+1}$, $|q| \ll 1$ of the spherical Bessel and Hankel functions, and neglected terms $O(k^2r^2)$ compared to 1. Similarly, for low-frequency response of a mounted vector sensor to an incident plane wave Eqs. (2), (3), and (5) give

$$v_r = \frac{-D}{\rho c}\left[e^{-ikr\cos\theta}\cos\theta + \frac{A_0}{k^2r^2} - \frac{6iA_1\cos\theta}{k^3r^3} - \frac{45A_2}{2k^4r^4}(3\cos^2\theta - 1)\right], \tag{10}$$

$$v_t = \frac{D\sin\theta}{\rho c}\left(e^{-ikr\cos\theta} + \frac{3iA_1}{k^3r^3} + \frac{45A_2}{k^4r^4}\cos\theta\right). \tag{11}$$

In Eqs. (9)–(11) and in all low-frequency expansions in the remainder of Sec. 2, we retain the dominant term and first-order corrections while discarding second- and higher-order terms.

Terms with scattering amplitudes A_n in Eqs. (9)–(11) describe the distortions of the low-frequency ambient field. For a mounted hydrophone, the monopole (isotropic) component of the scattered field with the amplitude A_0 dominates, and the dipole component with the amplitude A_1 provides first-order, i.e., $O(kr)$, corrections to the signal but not the ambient noise in Eq. (9). For the tangential velocity sensor, the dipole component dominates the distortions in Eq. (11), and linear corrections are due to the second spherical harmonic of the scattered field. For the radial velocity sensor, the dipole component again dominates the distortions in Eq. (10), and linear corrections are due to terms with A_0 and A_2, except for acoustically compliant floats with $Ms^2 \ll 1$. In the latter case, resonance scattering may occur, as discussed above. At frequencies close to the Minnaert resonance, the isotropic component of the scattered wave, which is represented by the term A_0/k^2r^2 in the square brackets in Eq. (10), dominates response of the sensor.

In the particular case of a sensor mounted on a rigid sphere, which corresponds to the limit $M \to \infty$ in Eqs. (4) and (5), $A_0 \approx ik^3a^3/3$, $A_1 \approx -ik^3a^3/6$ at low frequencies. Equation (9) shows then that the rigid sphere introduces negligible distortions in pressure measurements; v_r in Eq. (10) vanishes at $r=a$, as expected, and v_t in Eq. (11) is enhanced by the factor 1.5 relative the ambient field. For comparison, a sensor flush-mounted on a rigid plane records double the free-field acoustic pressure and tangential velocity.[1] Reflection from a plane serves also as the high-frequency limit of sound scattering by a sphere at points close to its surface.

In another particular case of a "soft" sphere with a pressure-release surface, which corresponds to the limit $M \to 0$ in Eqs. (4) and (5), $A_0 \approx ika(1+ika)$, $A_1 \approx ik^3a^3/3$. Then Eq. (9) gives $|p^2| = |D^2|(1-a/r)^2 + O(k^2r^2)$ for both the plane-wave response and measurements of diffuse noise. As expected, measured pressure as well as tangential velocity v_t in Eq. (11) vanish when $r \to a$, i.e., when the sensor approaches the pressure-release surface. According to Eq. (10), radial velocity amplitude is amplified by the large factor $1/kr$ relative to its ambient value. For comparison, normal velocity amplitude doubles near a pressure-release plane.[1]

These examples show that, depending on the material parameters of a float, its effect on performance of a mounted sensor spans the range from negligible to

drastic, even when the float is small compared to the wavelength of sound, has a non-trivial frequency dependence, and differs qualitatively from the effect of an infinite plane interface with the same boundary conditions.

3. Response of mounted sensors to distant sound sources and diffuse noise

Let an acoustic sensor be situated in a vicinity of a spherical float and away from the ocean surface and seafloor. Response of the sensor to a signal from a source in the far field can be modeled with plane-wave theory of Sec. 2. Response of a mounted sensor to an incident plane wave scales with sound frequency and float dimensions, and can be characterized by the dimensionless parameters $ka = \omega a/c$, M, s, r/a as well as the angle θ between the directions towards the source and the sensor from the center of the sphere. In analyzing the scattered wave effect on sensor response, we will use Eqs. (1)–(4), (7), (8) and focus on two widely used floatation types: thin-walled (usually glass), gas-filled floats, or GF for brevity, and syntactic foam, or SF, floats. Neglecting shear rigidity, these will be modeled as homogeneous fluids with $M = 0.013$, $s = 2/9$, which are parameters of air at 10 atm pressure, and $M = 0.5$, $s = 1.5$, respectively.

For the GF float, $Ms^2 \ll k^2a^2$ even at $ka = 0.1$. Then, according to Eq. (5), the low-frequency scattered wave is similar to that from a sphere with pressure-release boundary. Indeed, Fig. 1(b) shows a strong suppression by more than 25 dB of the field on a flush-mounted hydrophone and more than 15 dB for a hydrophone at the distance of $0.2a$ from the float. Zeroth spherical harmonic dominates in the incident wave and full field at low frequencies, leading to the weak angular dependence of the measurement distortion. As frequency increases, higher harmonics become progressively more important, leading to stronger angular dependence, but pressure on the mounted hydrophone remains strongly suppressed for all source bearings at $ka = 0.25$ [Fig. 1(b)]. When $ka \sim 1$ or larger, the position dependence of the phase difference between the incident and scattered waves is no longer negligible, and the signal suppression can be stronger on an offset hydrophone than on a flush-mounted one [Fig. 1(b)]. For a syntactic-foam-type float, low-frequency pressure distortions on a mounted sensor are much weaker than for a GF float and are only marginally sensitive to the hydrophone placement or source bearing [Fig. 1(c)]. Weak perturbations of the low-frequency plane-wave response translate into equally weak distortion of the ambient isotropic noise power spectrum when measured by a hydrophone mounted on the SF float or a platform with an even higher density [Fig. 1(d)].

Power spectrum measurements with a hydrophone mounted on a GF float lead to dramatic distortions varying from –43 to 27 dB in the frequency range of Fig. 1(d). Strong enhancement of the acoustic pressure occurs at resonances, which manifest as sharp peaks in Fig. 1(d) and exist at $ka < 1$ when either $Ms^2 \ll 1$ (for the fundamental, or Minnaert, resonance) or $s \ll 1$ (for higher-order resonances).[15] [In Fig. 1(b), frequencies are chosen to be away from the resonances.] The degree of destructive interference between the incident and scattered waves is sensitive to the sensor position and, at low frequencies, is typically stronger for a flush-mounted hydrophone than for an offset one [Fig. 1(d)]. While non-resonant features are virtually unaffected by dissipation, sound absorption in the float, which was modeled in Fig. 1(d) by multiplying the sound speed in the float by the factor $1–0.01i$, greatly reduces the effects of higher-order resonances. The strong suppression of the mounted hydrophone response at frequencies above the fundamental resonance is the reciprocal counterpart of the broadband suppression of low-frequency sound radiation[17] by sources in a vicinity of a compliant object. Enhancement of the low-frequency hydrophone response at the Minnaert resonance occurs in a wide range of float sound speeds and densities [Fig. 1(e)] as long as the resonance condition[12,15] $k^2a^2/3 = Ms^2 \ll 1$ is met. Figures 1(d) and 1(e) suggest that by changing platform parameters, such as increasing air pressure in a thin-walled float, one can increase mounted hydrophone sensitivity by 10 dB or more above its free-field level in a desired narrow frequency band.

Directivity of mounted radial and tangential velocity sensors is close to their free-field directivity at frequencies away from the resonances of float vibrations [Figs. 2(a), 2(b)]. However, because the radial velocity is amplified and tangential velocity is attenuated, the directivity will differ considerably from the free field for a single-axis sensor with any other orientation and for a tri-axial system. At low frequencies, as discussed in Sec. 2, the $n = 1$ spherical harmonic (i.e., the dipole component) dominates in the scattered field away from resonances. When $Ms^2 \ll 1$, the $n = 0$ (monopole) harmonic becomes significant and distorts the $|\cos\theta|$ angular dependence of the radial velocity sensor response. In the vicinity of the Minnaert resonance, the monopole component dominates and leads to strong amplification of

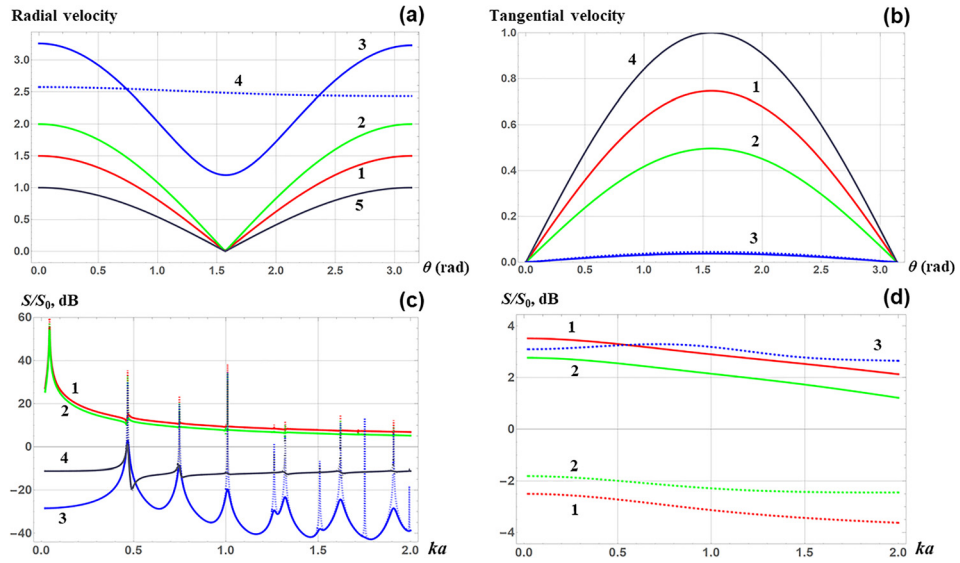

Fig. 2. (Color online) Response of a mounted vector sensor. (a) Dependence of the amplitude of the radial component of oscillatory velocity on the angle θ between the directions to a distant source and to the sensor from the platform center, for $ka = 0.1$, $r = a$, and various physical parameters of the float: $M = 0.5$ (curve 1), 0.25 (2), 0.013 (3) with $s = 1.5$. On curve 4, $M = 0.013$ and $s = 2/9$. The velocity amplitude is divided by 5 in this case to fit the line in the plot. For comparison, line 5 shows the ambient radial velocity amplitude. (b) Same as (a) but for the tangential component of oscillatory velocity at the sensor location for $ka = 0.2$ and $r = a$. Float parameters are $M = 0.5$, $s = 1.5$ (curve 1), $M = 0.25$, $s = 1.5$ (2), $M = 0.013$, $s = 1.5$ (3, solid line), and $M = 0.013$, $s = 2/9$ (3, dashed line). Curve 4 shows tangential velocity amplitude in the ambient field. (c) Frequency dependence of the ratio of measured and ambient power spectra of isotropic noise received by a velocity sensor in the vicinity of gas-filled float ($M = 0.013$, $s = 2/9$) with (solid lines) and without (dotted lines) account for sound absorption in the float. Curves 1–2 and 3–4 refer, respectively, to the radial and tangential channels of the velocity sensor that is located either at $r = a$ (curves 1 and 3) or $r = 1.1a$ (curves 2 and 4). (d) Same as (c) but for a syntactic-foam-type float ($M = 0.5$, $s = 1.5$; curves 1 and 2) or a heavier platform ($M = 10$, $s = 1.5$; curve 3). Solid and dashed lines refer to the radial and tangential channels, respectively, of the velocity sensor that is located either at $r = a$ (curves 1 and 3) or $r = 1.1a$ (curves 2).

the radial velocity [see lines 3 and 4 in Fig. 2(a)], while tangential velocity remains unaffected [see lines 3 in Fig. 2(b)].

The role of resonances is further illustrated in Fig. 2(c) for the GF float. In addition to the fundamental (Minnaert) resonance, in the absence of dissipation the radial velocity response exhibits a number of sharp peaks at higher-order resonances of the $n = 0$ harmonic as well as at resonances of harmonics $n = 1$–5. As expected, the tangential-velocity-component response peaks at the resonances of harmonics other than $n = 0$. Much like in the hydrophone case [Fig. 1(d)], effects of resonances other than the Minnaert one are greatly suppressed even by weak sound absorption [Fig. 2(c)]. Overall, radial velocity response is strongly enhanced, while tangential velocity response is strongly suppressed for a sensor in the vicinity of GF float, and the effect tends to gradually decrease with increasing sensor offset. For the SF float, there are no low-frequency resonances and no sensitivity to weak absorption, frequency dependence of vector sensor output is more gradual, and the measurement distortions are much lower than in the GF float case [see lines 1 and 2 in Fig. 2(d)]. Still, radial velocity is amplified, and tangential velocity is attenuated at $M = 0.5$. This is not necessarily the case for heavier platforms. With the density ratio increasing to $M = 10$ and the other parameters kept constant, the radial velocity component becomes attenuated by about 17 dB on the mounted sensor, while the tangential component is enhanced [line 3 in Fig. 2(d)].

Note that low-frequency measurement distortions by mounted vector sensors are systematically larger than by a hydrophone [cf. Figs. 1(b)–1(e) and Fig. 2]. That is ultimately due to a difference in the representative spatial scales between the incident and scattered waves in the vicinity of a platform. These scales are the wavelength $\lambda = 2\pi/k$ and $r \sim a \ll \lambda$, respectively. Hence, effects of the platform on the pressure gradient and oscillatory velocity are typically $(ka)^{-1} \gg 1$ times larger than on the acoustic pressure.

With a single mounted sensor, measurement distortions can be compensated for and the ambient (free-field) values of acoustic quantities retrieved using Eqs. (1)–(3), if mechanical parameters of the platform, including sound absorption, as well as the source bearing are known precisely. Much more practical approximate

corrections, which do not require any *a priori* information about the incident wave, can be obtained at low frequencies. As discussed in Sec. 2, the dipole component of the scattered wave dominates in the tangential velocity near a spherical platform as long as $kr \ll 1$. With the scattering amplitude $A_1 \approx ik^3a^3(1-M)/(1+2M)$ from Eq. (5), for the ratio of the received, v_t, and ambient, v_{t0}, values of the tangential velocity we find

$$\frac{v_t}{v_{t0}} \approx 1 + \frac{M-1}{2M+1}\frac{a^3}{r^3} \tag{12}$$

from Eq. (11) [cf. Figs. 2(b)–2(d)]. Similarly, for the non-resonance component of the radial velocity, from Eq. (10) we find [cf. Figs. 2(a), 2(d)]

$$\frac{v_r}{v_{r0}} \approx 1 - 2\frac{M-1}{2M+1}\frac{a^3}{r^3}. \tag{13}$$

In the case of highly compliant floats with $Ms^2 \ll 1$, the Minnaert resonance exists, and Eq. (13) applies only away from the resonance frequency. Scattering (diffraction) of sound enhances the tangential and suppresses radial velocity signal on a mounted vector sensor when $M>1$. The effect of diffraction on each of the components is opposite when $M<1$. Since one component is suppressed when the other is enhanced, the measured direction of particle velocity substantially differs from the ambient one, unless $r \gg a$. One needs to apply corrections Eqs. (12) and (13) to recover the source bearing from the vector sensor measurements.

4. Conclusion

It is sometimes argued, incorrectly, that the spatial scale of acoustic field variation is on the order of wavelength, and therefore small probes do not distort the ambient field. In fact, diffraction can significantly affect low-frequency acoustic fields in a vicinity of a compact object even when the object is small compared to the wavelength. We have shown that strong, frequency-dependent pressure perturbations occur in the vicinity of a small sphere when its compressibility is large compared to that of water. This leads to strong distortions in measurements when a hydrophone is placed near floats that employ thin, gas-filled shells. On the other hand, floats made of syntactic foam-type materials create only modest distortions of the free-field, low-frequency acoustic pressure values. Frequency dependence of the measurement distortions that occur on compact platforms proves to be rather different than in the previously studied limit of platforms that are large compared to wavelength.

Distortion of the ambient acoustic field by a sensor platform does not necessarily degrade the sensor performance. When understood and accurately modeled, amplitude distortions can be exploited to increase sensor sensitivity in a desired frequency band. Low-frequency phase distortions can be exploited to improve source bearing estimates.[18]

Scattering-induced low-frequency perturbations in oscillatory velocity and acceleration are generally much larger than pressure perturbations in the vicinity of sub-wavelength objects, leading to strong distortions of vector sensor measurements. Distortions of measurements of the tangential to the platform and normal components of oscillatory velocity by mounted vector sensors prove to be rather different. As a result, mounted vector sensors correctly measure neither the direction nor amplitude of the free-field oscillatory velocity. We have shown, however, that, away from resonances, the scattering-induced distortions in low-frequency vector sensor measurements can be readily corrected for, without any *a priori* information about the ambient acoustic field.

Acknowledgments

The author is grateful to Dr. A.B. Baynes and B.A. Cray for the benefit of our discussions and to anonymous reviewers for helpful suggestions. This work was supported by NSF Grant No. OCE1657430 and ONR Award No. N00014-19-WX-00462.

References and links

[1]D. Ross, *Mechanics of Underwater Noise* (Pergamon, New York, 1976), pp. 38–42, 184–196.

[2]S. H. Ko and A. H. Nuttal, "Analytical evaluation of flush-mounted hydrophone array response to the Corcos turbulent wall pressure spectrum," J. Acoust. Soc. Am. **90**(1), 579–588 (1991).

[3]S. H. Kim, S. Y. Hong, J. H. Song, H. G. Kil, J. J. Jeon, and Y. S. Seo, "Acoustical characteristic predictions of a multi-layer system of a submerged vehicle hull mounted sonar simplified to an infinite planar model," Int. J. Naval Architecture Ocean Eng. **4**(2), 96–111 (2012).

[4]F. K. Duennebier and G. H. Sutton, "Fidelity of ocean bottom seismic observations," Marine Geophys. Res. **17**(6), 535–555, https://doi.org/10.1007/BF01204343 (1995).
[5]M. Hawkes and A. Nehorai, "Acoustic vector-sensor processing in the presence of a reflecting boundary," IEEE Trans. Signal Proc. **48**(11), 2981–2993 (2000).
[6]K. B. Smith, "Effects of shear waves on boundary-coupled vector sensors," J. Acoust. Soc. Am. **124**(6), 3464–3470 (2008).
[7]Y. I. Wu, S. K. Lau, and K. T. Wong, "Near-field/far-field array manifold of an acoustic vector-sensor near a reflecting boundary," J. Acoust. Soc. Am. **139**(6), 3159–3176 (2016).
[8]O. A. Godin, N. A. Zabotin, and V. V. Goncharov, "Ocean tomography with acoustic daylight," Geophys. Res. Lett. **37**(13), L13605, https://doi.org/10.1029/2010GL043623 (2010).
[9]K. F. Woolfe, S. Lani, K. G. Sabra, and W. A. Kuperman, "Monitoring deep-ocean temperatures using acoustic ambient noise," Geophys. Res. Lett. **42**(8), 2878–2884, https://doi.org/10.1002/2015GL063438 (2015).
[10]M. G. Brown, O. A. Godin, X. Zang, J. S. Ball, N. A. Zabotin, L. Y. Zabotina, and N. J. Williams, "Ocean acoustic remote sensing using ambient noise: Results from the Florida Straits," Geophys. J. Int. **206**, 574–589 (2016).
[11]T. Akal and J. M. Berkson, *Ocean Seismo-Acoustics: Low-Frequency Underwater Acoustics* (Plenum, New York, 1986).
[12]V. C. Anderson, "Sound scattering from a fluid sphere," J. Acoust. Soc. Am. **22**, 426–431 (1950).
[13]A. G. Pathak and P. R. Stepanishen, "Acoustic harmonic radiation from fluid-loaded spherical shells using elasticity theory," J. Acoust. Soc. Am. **96**(4), 2564–2575 (1994).
[14]R. J. Barton, K. B. Smith, and H. T. Vincent, "A characterization of the scattered acoustic intensity field in the resonance region for simple spheres," J. Acoust. Soc. Am. **129**(5), 2772–2784 (2011).
[15]O. A. Godin, "Rayleigh scattering of a spherical sound wave," J. Acoust. Soc. Am. **133**(2), 709–720 (2013).
[16]M. Abramovitz and I. A. Stegun, *Handbook of Mathematical Functions with Formulas, Graphs, and Tables*, Vol. 55 of Applied Mathematics Series (Dover Publications, New York, 1972), pp. 355–442.
[17]O. A. Godin and A. B. Baynes, "Passive, broadband suppression of radiation of low-frequency sound," J. Acoust. Soc. Am. **143**(2), EL67–EL73 (2018).
[18]A. B. Baynes and O. A. Godin, "Rayleigh scattering of a cylindrical sound wave by an infinite cylinder," J. Acoust. Soc. Am. **142**(6), 3613–3623 (2017).